

# Step Height Calibration Using Hamming Window Band-Pass Filter

Dahi Ghareab Abdelsalam Ibrahim

**Abstract**—Axial and lateral measurements of a step depth standard are presented. The axial measurement is performed based on the ISO 5436 profile analysis. The lateral measurement is performed based on the Hamming window band-pass filter method. The method is applied to calibrate a groove structure of a step depth standard of 60 nm. For the axial measurement, the computed results show that the depth of the groove structure is  $59.7 \pm 0.6$  nm. For the lateral measurement, the computed results show that the difference between the two line edges of the groove structure is  $151.7 \pm 2.5$  nm. The method can be applied to any step height/depth regardless of the sharpness of the line edges.

**Keywords**—Hamming window, band-pass filter, metrology, interferometry.

## I. INTRODUCTION

STEP height/depth standards refer to precise measurements used to calibrate or verify the accuracy of instruments and systems designed to measure vertical distances. Step height/depth standards are needed for various applications in length metrology [1], [2]. The axial scale of the atomic force microscope (AFM) and stylus instruments is calibrated by a calibrated step height standard [3]. Step height/depth standards are calibrated by the interference microscope traceable to the SI unit through stabilized wavelengths [4], [5]. Following the ISO 5436 profile analysis [6], the axial height/depth can be measured precisely. For groove structures, for example, the axial depth is measured by averaging the depths at the active measurement areas at the edges minus the average depth at the active measurement area at the groove. The ISO 5436 profile analysis does not provide a direct method for the lateral measurements of the step height/depth standards. In this paper, the Hamming window pass-band filter is used to compute the lateral measurements of the step height/depth standards. Lateral measurements of the step height/depth standards are a crucial measure for many applications in the industry [7]-[11]. In the lateral measurements, the experimental profile of the step height/depth is simulated by the Hamming window pass-band filter. The lateral position of 50% height/depth value of the mimicked Hamming profile is assigned. The areas up and down the assigned value of the line edges of the step/depth are then computed and compared. The difference between the areas of the two line edges is the lateral measurement of the step height/depth standard. In this paper, we applied the Hamming window pass-band filter to improve the axial measurements and compute the lateral measurements of a groove structure with a nominal depth standard of 60 nm.

Dahi Ghareab Abdelsalam Ibrahim is with the Engineering and Surface Metrology Lab., National Institute of Standards, Tersa St., El haram, El Giza,

The experimental profile of the groove structure is extracted from the reconstruction of two shots captured from a common-path phase-shift microscope [12]. The microscope is based on the measurement of the Stokes parameters  $S_2$  and  $S_3$ . The Stokes parameters describe the polarized light incident to the camera. The temporal stability of the microscope is down to 1.3 nm for one hour. Experimental results show that the axial depth of the groove structure is  $59.7 \pm 0.6$  nm, which is very closely to the nominal value. The computational results show that the lateral measurement, which is the difference between the two line edges of the groove structure, is  $151.7 \pm 2.5$  nm.

## II. HAMMING WINDOW MODEL

A window function is used to analyze a small part of a signal. There are many available types of window functions frequently used. Such windows are the rectangular window, the Bartlett window, the Gaussian window, the Blackman window, the flat-top window, and the Hamming window. Each window has its advantages and drawbacks. Here, we used the Hamming window that can be used as a band-pass filter by multiplying it with a signal in the frequency domain. Band-pass filters are used to permit a range of frequencies within a lower and upper threshold. This effectively removes low-frequency components and high-frequency components, leaving only the frequencies in the desired band. The Hamming window: pass-band filter is expressed as [13], [14]:

$$w_H(n) = 0.54 - 0.46 \cos\left(\frac{2\pi n}{N-1}\right), \quad (1)$$

where  $n \in \{0, \dots, N-1\}$  and  $N$  is the filter order. Fig. 1 shows the weighting function of the Hamming window when an original waveform of  $y = \sin(2\pi t/100)$  with  $t = (0: 500)$  passes through it. The weighting function of the Hamming window  $w = \sin(2\pi t/100)$ . \* window (@hamming, 501). The discrete-time Fourier transform (DTFT) of the sequence  $2h(n)\cos(2\pi n f_0) = h(n)e^{2j\pi n f_0} + h(n)e^{-2j\pi n f_0}$  can be written as  $H(f - f_0) + H(f + f_0)$  where  $h$  is the impulse response, and  $f_0$  is the cut-off frequency. Here, one component of  $H(f - f_0)$  or  $H(f + f_0)$  is selected. Hence, if  $H(f)$  is the complex gain of a low-pass filter, the result is a filter the complex gain of which is centered around  $\pm f_0$ , therefore a band-pass filter. To maintain a linear phase, a  $2 \cos(2\pi n f_0)$  is multiplied if  $N$  is odd and is multiplied if  $N$  is even. For  $N$  odd, the impulse response  $h(n)$  is expressed as:

Egypt (e-mail: dahi.abdelsalam@nis.sci.eg).

$$h(n) = \int_{-f_0}^{f_0} e^{2jmf} df = \frac{\sin(2\pi n f_0)}{\pi n}, \quad (2)$$

and for  $N$  even, the impulse response  $h(n)$  is expressed as:

$$h(n) = \int_{-f_0}^{f_0} e^{j\pi f} e^{2jmf} df = \frac{\sin(2\pi(n+0.5)f_0)}{\pi(n+0.5)}. \quad (3)$$

The simulated gain spectrum (abs  $(2 h(n) \cos(2\pi n f_0))$ ) by the Hamming window band-pass filter for a line structure at  $f_0 = 0.25$ ,  $f_b = 0.12$ , and  $N = 981$  is shown in Fig. 2 (a).

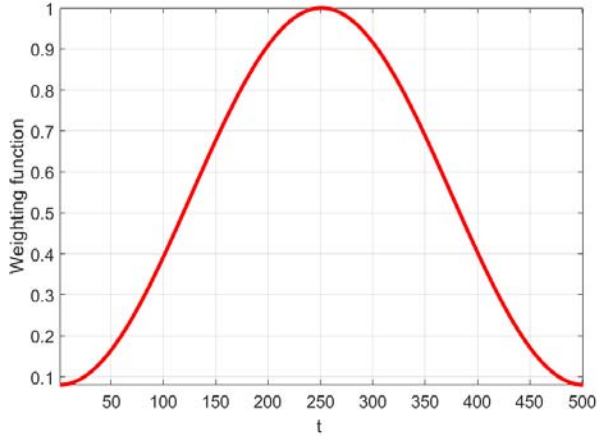


Fig. 1 The weighting function of the Hamming window  $w = \sin(2\pi t/100)$ ; \* window (@hamming, 501); t is a number

Fig. 2 (b) shows a simulated gain spectrum of a groove structure with the Hamming window band-pass filter at cut-off frequency = 0.25,  $f_b = 0.12$ , and filter order = 881. Here, the  $f_b$  is responsible for widening or narrowing the width of the gain.

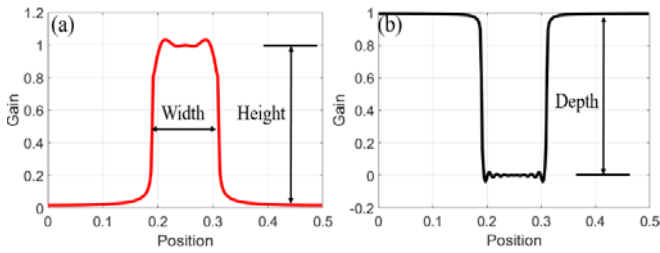


Fig. 2 (a) Mimicked gain spectrum of a line structure with the Hamming window band-pass filter at  $f_0 = 0.25$ ,  $f_b = 0.12$ , and filter order  $N = 981$ ; (b) Mimicked gain spectrum of a groove structure with the Hamming window band-pass filter at  $f_0 = 0.25$ ,  $f_b = 0.12$ , and  $N = 881$

As seen in Fig. 2, the gain (vertical axis) of the mimicked profile ranges from 0 to one should be rescaled to fit the experimental axial scale. Also, the position (horizontal axis) should be rescaled to fit the length (or via the number of pixels) of the horizontal experimental profile.

### III. EXPERIMENT

The schematic diagrams of the optical systems used to extract the experimental profile of the object, which is a groove

structure of a transparent step depth standard of a nominal axial depth of 60 nm and a lateral nominal width of 200  $\mu\text{m}$  are shown in Figs. 3 (a) and (b). The object is made by plating chrome on a soda-lime glass substrate. The optical system is a common-path phase-shift microscope based on the measurement of the Stokes parameters  $S_2$  and  $S_3$  [12]. Fig. 3 (a) is used to extract  $S_{2R}$  and  $S_{3R}$  in the absence of the object, while Fig. 3 (b) is used to extract  $S_{2T}$  and  $S_{3T}$  in the presence of the object. The optical system can be regarded as a combination of Zernike's phase contrast microscopy, which delivers high-contrast intensity images of transparent specimens, and Gabor's holography, where the phase information from the object is recorded. The optical system works by phase shifting technique for precise measurement with an error of  $\lambda/100$  [15].

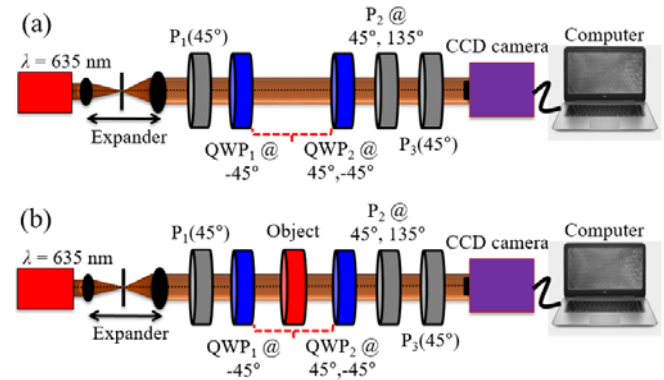


Fig. 3 Schematic diagram of the common-path optical phase shift system (a) without the object and (b) with the object; P1 (45°) is a polarizer fixed at 45°; P2 @ 45°, 135° is a polarizer rotated at 45° and 135° for obtaining the  $S_{2R}$  and  $S_{2T}$ ; QWP1 @ -45° is a quarter wave plate fixed at -45°; QWP2 @ 45°, -45° is a quarter wave plate rotated at 45° and -45° for obtaining the  $S_{3R}$  and  $S_{3T}$

The optical system does not employ a PZT phase shifter to avoid the nonlinear response of the PZT to the applied voltage and the thermal drift in the PZT. Moreover, since it is a common-path scheme, it reduces the effects of mechanical vibrations and air turbulence, which are the fundamental error sources in interferometric measurements. A calibrated laser diode of  $\lambda = 635$  nm is connected to a collimation and beam size expansion section which comprises a length extendable tube and a plano-convex lens of 30 mm diameter. A shearing interferometer was used to achieve good collimation. The collimated beam is directed to three polarizers (P1 (45°), P2 @ 45°, 135°, P3 (45°)), two QWPs, the object being measured, and a CCD camera (1600 pixels horizontal by 1200 pixels vertical, with unit cell dimension of 4.4  $\mu\text{m}$  square). The three polarizers and the two QWPs were calibrated using a commercial Thorlabs polarimeter. The light is linearly polarized by a polarizer P1 (set at an azimuth angle  $\theta = 45^\circ$ ). The linear polarized light passes through a QWP1 (set at an azimuth angle  $\theta = -45^\circ$ ). The beams exit from the object are two: one remains un-scattered and forms a uniform background of the image and the other is scattered and contains the fine structure information of the object. To extract the phase image of the object ( $\Delta_{Obj}$ ), a reference phase image ( $\Delta_{Ref}$ ) in the absence of the object is

extracted and then subtracted from the total phase image ( $\Delta_T$ ) in the presence of the object. To extract ( $\Delta_{Ref}$ ) and ( $\Delta_T$ ), the  $S_{2R}$ ,  $S_{2T}$ ,  $S_{3R}$ , and  $S_{3T}$  should be computed.

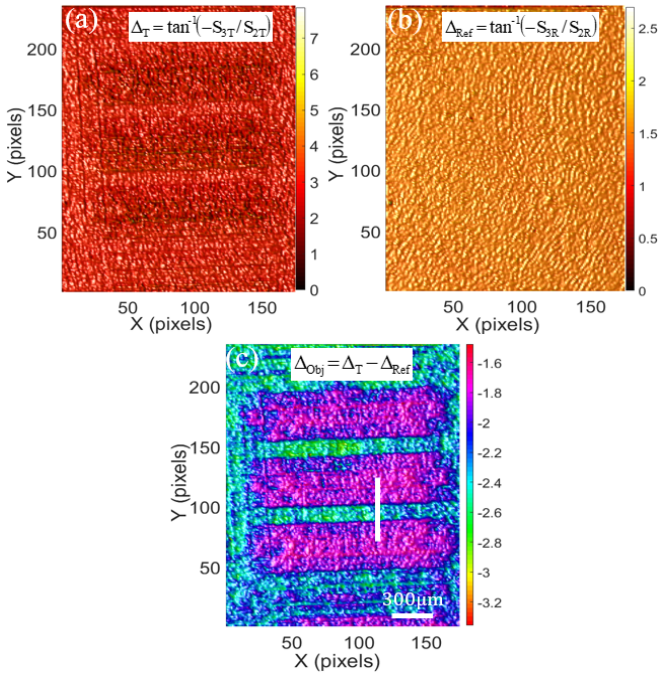


Fig. 4 (a) Experimental  $\Delta_T$ ; (b) Experimental  $\Delta_{Ref}$ ; (c) Extracted  $\Delta_{Obj}$

The  $S_{2R}$  and  $S_{2T}$  in the absence and in the presence of the object being measured are computed with no use of QWP<sub>2</sub>, and by rotating the polarizer  $P_2$  at  $45^\circ$  and  $135^\circ$ , the intensity images  $I_{45T}$  and  $I_{135T}$  are captured by the CCD camera. The difference between the two intensity images in the absence of the object is  $S_{2R} = (I_{45R} - I_{135R})$ . In the same manner, the difference between the two intensity images in the presence of the object is  $S_{2T} = (I_{45T} - I_{135T})$ .

The  $S_{3R}$  and  $S_{3T}$  in the absence and in the presence of the object being measured are computed using the QWP<sub>2</sub>, keeping the polarizer  $P_2$  fixed at  $45^\circ$ , like  $P_1$  and  $P_3$ . By rotating the QWP<sub>2</sub> at  $45^\circ$  (RHC) and  $-45^\circ$  (LHC), two intensity images,  $I_{LHC}$  and  $I_{RHC}$ , are captured by the CCD camera. The difference between the two intensity images in the absence of the object is  $S_{3R} = (I_{LHCR} - I_{RHCR})$ . The difference between the two intensity images in the presence of the object is  $S_{3T} = (I_{LHCT} - I_{RHCT})$ . The reference phase image ( $\Delta_{Ref}$ ) is computed from the  $S_{2R}$  and  $S_{3R}$  as follows [12]:

$$\Delta_{Ref} = \tan^{-1}(-S_{3R}/S_{2R}). \quad (4)$$

The total phase image ( $\Delta_T$ ) which includes the reference phase ( $\Delta_{Ref}$ ) and the object phase ( $\Delta_{Obj}$ ) is computed from the  $S_{2T}$  and  $S_{3T}$  as:

$$\Delta_T = \tan^{-1}(-S_{3T}/S_{2T}). \quad (5)$$

The phase image of the object ( $\Delta_{Obj}$ ) is computed via

subtraction of the reference phase ( $\Delta_{Ref}$ ) from the total phase ( $\Delta_T$ ) as:

$$\Delta_{Obj} = \Delta_T - \Delta_{Ref}. \quad (6)$$

Figs. 4 (a) and (b) show the experimental  $\Delta_T$  and  $\Delta_{Ref}$ , respectively.

#### IV. AXIAL MEASUREMENT OF THE STEP DEPTH STANDARD

Fig. 4 (c) shows the reconstructed phase image of the groove structure of a transparent step depth standard of a nominal depth of 60 nm and a lateral nominal width of 200  $\mu\text{m}$  using (6) after unwrapping using the graph cuts method [16]. A cut line along the white line of Fig. 4 (c) is extracted and shown in the blue phase profile in Fig. 6. Note that the experimental phase profile occupies a horizontal distance of 70 pixels in the y direction, so the mimicked Hamming profile should be rescaled to fit the experimental horizontal distance. The experimental profile is divided into five regions as shown in Fig. 5. According to the ISO 5436 profile analysis [6], the height/depth measurements are computed using regions 1, 3, and 5 by averaging the heights/depths at the active measurement areas 1 and 5 minus the average height/depth at the active measurement area 3. Since the ISO 5436 profile analysis does not present a method for lateral measurements of step height/depth standards, the Hamming area model is proposed in this article to measure the lateral measurements using regions 2 and 4. As seen in Fig. 5, the noise vibration in the phase profiles of regions 1, 3, and 5 varies like a sinusoidal function; thus, phase error ( $p_{rms}$ ) can be expressed as the root mean square (RMS) value of the disturbed phase. The RMS phase error can be expressed as:

$$p_{rms} = \sqrt{[p - \bar{p}]^2 / (\aleph - 1)}, \quad (7)$$

where  $p$  stands for the phase distribution,  $\bar{p}$  denotes the mean values, and  $\aleph$  represents the pixel number of the experimental profile. The modified blue profile by applying the RMS model is shown in the red profile in Fig. 5.

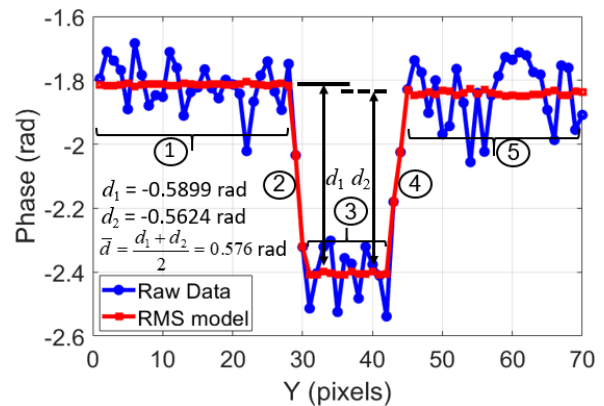


Fig. 5 Experimental phase profile (blue) along the white line of Fig. 4 (c) before applying the RMS model and after applying the RMS model (red profile)

The standard deviation is used to quantify the error before and after applying the RMS model. The standard deviation of region 1 in Fig. 5 is calculated to be  $\sigma_{Raw} = 0.072$  rad, while the standard deviation of the red profile is calculated to be  $\sigma_{RMS} = 0.003$  rad. The difference between  $\sigma_{Raw}$  and  $\sigma_{RMS}$  of region 1 in Fig. 5 is calculated to be  $\sigma_{diff} = 0.072 - 0.003 = 0.069$  rad i.e. depth error =  $(0.069 \times 635)/(2\pi) \cong 7$  nm. In the same manner, the standard deviation of region 5 in Fig. 5 is calculated to be  $\sigma_{Raw} = 0.103$  rad, while the standard deviation of the red profile is calculated to be  $\sigma_{RMS} = 0.007$  rad. The difference between  $\sigma_{Raw}$  and  $\sigma_{RMS}$  of region 5 in Fig. 5 is calculated to be  $\sigma_{diff} = 0.103 - 0.007 = 0.096$  rad i.e. depth error =  $(0.096 \times 635)/(2\pi) \cong 10$  nm. In the same manner, the standard deviation of the blue profile in region 3 of Fig. 5 is calculated to be  $\sigma_{Raw} = 0.085$  rad, while the standard deviation of the red profile is calculated to be  $\sigma_{RMS} = 0.004$  rad. The difference between  $\sigma_{Raw}$  and  $\sigma_{RMS}$  of region 3 in Fig. 5 is calculated to be  $\sigma_{diff} = 0.085 - 0.004 = 0.081$  rad i.e. depth error =  $(0.081 \times 635)/(2\pi) \cong 8$  nm. Note that the depth measurements have been carried out using the red profiles of Fig. 5 i.e. after applying the RMS model. The average standard deviation of the red profiles in regions 1, 5, and 3 is computed to be around 0.4 nm. Note also that the measurement noise is found experimentally to be around 0.07 nm for one-second data acquisition using a surface topography repeatability test. As seen in Fig. 5, the average phase is calculated to be 0.576 rad i.e. depth =  $(0.576 \times 635)/(2\pi) \cong 58.3$  nm. The sources of uncertainty [17-18] including the above-measured errors in addition to errors arising from the calibrated laser source and collimation have been estimated to be 0.6 nm, which is about 1% of the measured depth. Note that, by using the Hamming profile, the depth measurement is improved to be 0.589 rad i.e. depth =  $(0.589 \times 635)/(2\pi) \cong 59.7$  nm, which approaches very closely to the nominal value, which is 60 nm.

#### V. LATERAL MEASUREMENT OF THE STEP DEPTH STANDARD

The red profile in Fig. 6 shows the experimental phase profile after applying the RMS model, while the green color is the mimicked Hamming profile simulated at  $f_0 = 0.26$ ,  $f_b = 0.102$ , and  $N = 781$ . The Hamming horizontal axis in Fig. 6 is rescaled by multiplying a value of 140 to fit the scale of the experimental profile, while the Hamming vertical axis is rescaled by multiplying a value of 0.59 and the result is subtracted from 1.81 value to fit the experimental vertical scale. Note that the mimicked profile is adjusted on the experimental profile after applying the RMS not on the raw profile, which means better accuracy is achieved. As seen in Fig. 6, the sharpness of lateral measurements of the left line edge and right line edge is estimated via the Hamming area. We used the expression of Hamming area since the area is computed using the position of the 50% depth value ( $0.5d_{Ham}$ ) of the mimicked Hamming profile. As seen in Fig. 6, the left line edge includes two areas  $A_1$  and  $A_2$ , and the right line edge includes two areas  $A_3$  and  $A_4$ . The tips of  $A_1$  and  $A_4$  are down, while the tips of  $A_2$  and  $A_3$  are up. The two areas of the left line edge  $A_1$  and  $A_2$  are summed up and the result of summation is subtracted from the result of summation of the two areas of the right line edge  $A_3$  and  $A_4$ . By knowing the difference, a quantitative lateral reconditioning could be performed.

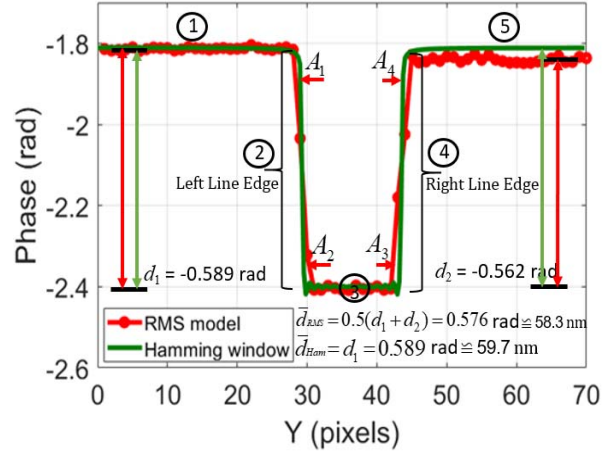


Fig. 6 Experimental phase profile (red color) after applying the RMS model, and its mimicked Hamming profile (green color)

Fig. 7 shows the shaded areas between the experimental and its mimicked profiles using a fill function in MATLAB. As seen in Fig. 7, the four lateral areas  $A_1$ ,  $A_2$ ,  $A_3$ , and  $A_4$  of the left line edge and the right line edge of the groove structure appear clearly with formed borders and with an assigned depth value of  $0.5d_{Ham}$ . The assigned point value  $0.5d_{Ham}$  is expressed as:

$$0.5d_{Ham} = (d_0 + d_{Ham} / 2) \quad (8)$$

The value of  $d_0$  is the average depth at the mimicked edges of regions 1 and 5. The value of  $d_0$  is found to be -1.8135 in Fig. 7, and  $d_{Ham}/2 = 0.5899/2 = 0.295$  rad. The assigned value  $0.5d_{Ham} = -1.8135 - 0.2950 = -2.1085$  rad.

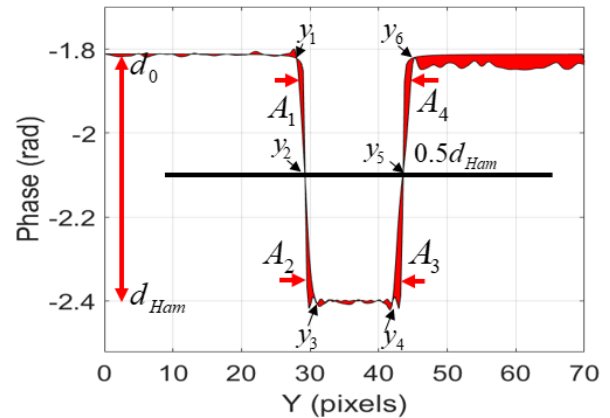


Fig. 7 Shaded areas between the experimental and its mimicked Hamming profiles using a fill function in MATLAB; appearance of the up and down areas  $A_1$ ,  $A_2$ ,  $A_3$ , and  $A_4$  for lateral measurements

As seen in Fig. 7, one can estimate by the naked eye that  $A_4 > A_1$  and  $A_3 > A_2$  or  $|A_3 + A_4| > |A_1 + A_2|$ , which means that the reconditioning process should be implemented on the right line edge to achieve symmetrical line edges of the groove structure. To quantify this value, the areas  $A_1$ ,  $A_2$ ,  $A_3$ , and  $A_4$  should be computed precisely.

The integrals of the shaded areas  $A_1$  and  $A_2$  of the left line edge up and down the assigned value of Fig. 7 are given as

follows:

$$A_1 = \int_{y_1}^{y_2} [d_{Exp}(y) - d_{Ham}(y)] dy, \quad (9)$$

$$A_2 = \int_{y_2}^{y_3} [d_{Exp}(y) - d_{Ham}(y)] dy. \quad (10)$$

The total area of the left line edge in Fig. 7 is expressed as:

$$Left\ Line\ Edge\ A_T = |A_1 + A_2|. \quad (11)$$

In the same manner, the integrals of the shaded areas  $A_3$  and  $A_4$  of the right line edge down and up the assigned value of Fig. 7 are given as follows:

$$A_3 = \int_{y_4}^{y_5} [d_{Exp}(y) - d_{Ham}(y)] dy, \quad (12)$$

$$A_4 = \int_{y_5}^{y_6} [d_{Exp}(y) - d_{Ham}(y)] dy. \quad (13)$$

The total area of the right line edge in Fig. 7 is expressed as:

$$Right\ Line\ Edge\ A_T = |A_3 + A_4|. \quad (14)$$

The difference (degree of symmetry) between the total area included in the right line edge and the total area included in the left line edge is expressed as:

$$\Delta A = Right\ Line\ Edge\ A_T - Left\ Line\ Edge\ A_T. \quad (15)$$

Here, we used the trapz function in MATLAB to integrate the data with unit spacing. For an integration with  $S+1$  evenly-spaced points, the approximate is expressed as follows [19]:

$$\int_a^b f(y) dy \approx \frac{b-a}{2S} \sum_{n=1}^S (f(y_n) + f(y_{n+1})), \quad (16)$$

where the spacing between each point is equal to the scalar value  $(b-a)/S$ , and this spacing equals one in MATLAB. When the spacing between the  $S+1$  points is not regular, then (16) generalizes to the following equation [19]:

$$\int_a^b f(y) dy = \frac{1}{2} \sum_{n=1}^S (y_{n+1} - y_n) [f(y_n) + f(y_{n+1})], \quad (17)$$

where  $a = y_1 < y_2 < \dots < y_S < y_{S+1} = b$ , and  $(y_{n+1} - y_n)$  is the spacing between each consecutive pair of points.

The approximate integrations of the four lateral areas  $A_1$ ,  $A_2$ ,  $A_3$ , and  $A_4$  using the trapz function in MATLAB yield values of -1.044 rad, -1.086 rad, -2.09 rad, and -1.54 rad, respectively.

The total area included in the left line edge is computed using (11) to be:  $|A_1 + A_2| = |-1.044 - 1.086| = |-2.13| = 2.13$  rad. Also, the total area included in the right line edge is computed using (14) to be:  $|A_3 + A_4| = |-2.09 - 1.54| = |-3.63| = 3.63$  rad. The difference (degree of symmetry) between the total area included in the right line edge and the total area included in the left line edge is computed using (15) to be:  $\Delta A = 3.63$  rad -  $2.13$  rad =  $1.5$  rad =  $(1.5 \times 635/2 \times \pi) = 151.66$  nm. This means that a reconditioning process should be applied to remove 151.66 nm from the right line edge to be symmetrical with the left line edge. More specifically, the value of 151.66 nm is distributed over the two included areas  $A_3$  and  $A_4$  in the right line edge as follows: the absolute difference in up areas  $A_1$  and  $A_4$  above the  $0.5d_{Ham}$  is expressed as  $|A_4 - A_1| = |-1.54 + 1.044| = 0.496$  rad =  $(0.496 \times 635/2 \times \pi) = 50.15$  nm. In the same manner, the absolute difference in down areas  $A_2$  and  $A_3$  below the  $0.5d_{Ham}$  is expressed as  $|A_3 - A_2| = |-2.09 + 1.086| = 1.004$  rad =  $(1.004 \times 635/2 \times \pi) = 101.51$  nm. This means that the reconditioning process should be applied to remove 50.15 nm from  $A_4$  and 101.51 nm from  $A_3$  to be symmetrical with the areas  $A_1$  and  $A_2$ , respectively. The error in area measurement by the trapz function was estimated by applying the trapz function to compute many simulated standard areas. For example, a standard area of 42 was computed by the trapz function to be 41.3, i.e. the error in area measurement is 1.7%. The 1.7% of 151.66 nm equals 2.5 nm. Table I shows the obtained results of areas  $A_1$ ,  $A_2$ ,  $A_3$ , and  $A_4$  of the groove structure computed with the trapz function.

TABLE I  
MEASUREMENT OF AREAS  $A_1, A_2, A_3,$  AND  $A_4$  OF THE GROOVE STRUCTURE

Left Line Edge		Right Line Edge	
Area	Computed value (rad)	Area	Computed value (rad)
$A_1$	-1.044	$A_3$	-2.09
$A_2$	-1.086	$A_4$	-1.54
$ A_1 + A_2 $	2.13	$ A_3 + A_4 $	3.63
$\Delta A =  A_3 + A_4  -  A_1 + A_2  = 3.63$ rad - $2.13$ rad = $1.5$ rad = $(1.5 \times 635/2 \times \pi) = 151.66$ nm			

Fig. 8 (a) shows the total area included in the left line edge, while Fig. 8 (b) shows the total area included in the right line edge. By the naked eye, one can estimate that the total area included in the right line edge is bigger than the total area included in the left line edge. By using the proposed Hamming area model, it is easy to compute the difference in area included in both line edges, which is 151.66 nm.

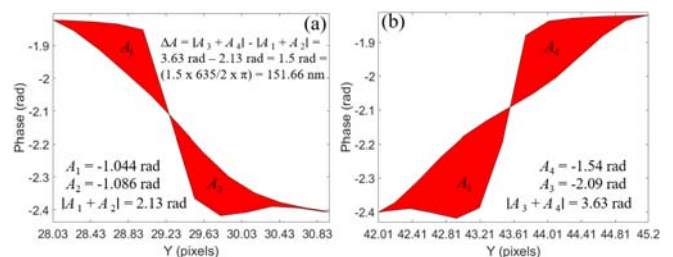


Fig. 8 (a) The total area included in the left line edge of Fig. 7; (b) The total area included in the right line edge of Fig. 7

## VI. CONCLUSION

In conclusion, a method based on the Hamming area model for precise lateral measurements of the line/groove structures has been presented. The lateral measurements of the step height/depth standards have many applications, especially in the fields of lithography and calibration of pixel cameras. The error in lateral area measurement by the proposed Hamming area model based on a trapezoidal integration has been computed to be 1.7%. The method improves the axial measurements of the line/groove structures by around 2.3%.

**Dahi Ghareab Abdelsalam Ibrahim** received his BS and MS in Physics from Minia University, Egypt, in 1997 and 2001, respectively. He holds a Ph.D. in Optical Metrology and is currently a Professor of Optical Metrology and a head of the Length and Engineering Precision Division at the National Institute of Standards, Egypt. He has published more than 75 peer-reviewed papers, one patent, three book chapters, and authored one book titled Optical Metrology with Interferometry.

## REFERENCES

- [1] Peter J. de Groot, "The meaning and measure of vertical resolution in optical surface topography measurement", *Applied Sciences*, 7, 54, 2017, pp. 2- 6.
- [2] ISO DIS 25178-600:201: Geometrical Product Specifications (GPS)-Surface Texture: Areal-Part 600: Metrological Characteristics for Areal-Topography Measuring Methods (DRAFT 2016-05-07); International Organization for Standardization: Geneva, Switzerland, 2016.
- [3] J. Garnaes, N. Kofod, A. Kühle, C. Nielsen, K. Dirscherl, L. Blunt, "Calibration of step heights and roughness measurements with atomic force microscopes," *Precision Engineering*, 27, 2003, pp. 91-98.
- [4] Jungjae Park, Yoon-Soo Jang and Jonghan Jin, "Length measurement based on multi-wavelength interferometry using numerous stabilized frequency modes of an optical comb," *Metrologia* 61, 2024, 015007 (8pp).
- [5] Nicolas Schuhler, Yves Salvadé, Samuel Lévêque, René Dändliker, and Ronald Holzwarth, "Frequency-comb-referenced two-wavelength source for absolute distance measurement", *Optics Letters*, 31, 2006, pp. 3101-3103.
- [6] ISO/TC 213, "Geometrical product specifications (GPS) – Surface texture: Profile method; Measurement standards - Part 2: Software measurement standards," ISO 5436, Edition: 2, Number of pages: 17, 2012.
- [7] Dahi Ghareab Abdelsalam Ibrahim, "Improving the intensity-contrast image of a noisy digital hologram by convolution of Chebyshev type 2 and elliptic filters", *Appl. Opt.* 60, 2021, pp. 3823-3892.
- [8] Andreas Fischer, Dirk Stobener, Gert Behrends, "A lateral-scanning white-light interferometer for topography measurements on rotating objects in process environments," *CIRP Annals - Manufacturing Technology*, 71, 2022, pp. 437-440.
- [9] de Groot P, "Principles of interference microscopy for the measurement of surface topography," *Adv Opt Photonics*, 7, 2015, pp:1-65.
- [10] You J, Kim S-W, "Optical inspection of complex patterns of microelectronics products," *CIRP Ann Manuf Technol*, 57, 2008, pp:505-508.
- [11] Dahi Ghareab Abdelsalam Ibrahim, "Estimation of an uncertainty budget and performance measurement for a dual-wavelength Twyman-Green interferometer," *J. Microsc.*, 2021, pp. 1-15.
- [12] Dahi Ghareab Abdelsalam Ibrahim, "Common-path phase-shift microscope based on measurement of Stokes parameters  $S_2$  and  $S_3$  for 3D phase extraction", *Appl. Opt.* 59, 2020, pp. 5779-5784.
- [13] Dahi Ghareab Abdelsalam Ibrahim, "Calibration of a step height standard for dimensional metrology using phase-shift interferometry and Hamming window: band-pass filter," *J Opt.* 2023, pp.1-9.
- [14] Gerard Blanchet, Maurice Charbit, "Digital signal and image processing using MATLAB," John Wiley & Sons, Inc., 2<sup>nd</sup> Edition, Volume 2, ISBN 978-1-84821-640-2, ISTE Ltd, 2014.
- [15] Y.-Y. Cheng and J. C. Wyant, "Two-wavelength phase-shifting interferometry," *Appl. Opt.* 23, 1984, pp. 4539.
- [16] J. M. Bioucas-Dias and G. Valadao, "Phase unwrapping via graph cuts," *IEEE Trans. Image Process.* 16, 2007, pp. 698-709.
- [17] JCGM 100:2008 Evaluation of Measurement Data-Guide to the Expression of Uncertainty in Measurement (GUM); Joint Committee for Guides in Metrology: Geneva, Switzerland, 2008.
- [18] Dahi Ghareab Abdelsalam Ibrahim, "Estimation of an uncertainty budget and performance measurement for a dual-wavelength Twyman-Green interferometer," *J Microsc.* 282, 2021, pp. 1-15.
- [19] <https://fr.mathworks.com/help/matlab/ref/trapz.html>